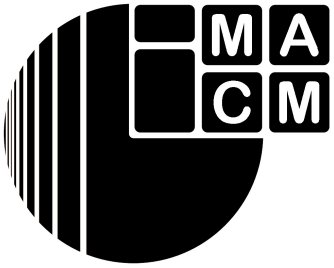


Bergische Universität Wuppertal

Fachbereich Mathematik und Naturwissenschaften

Institute of Mathematical Modelling, Analysis and Computational Mathematics (IMACM)

Preprint BUW-IMACM 15/08

M. Chraibi, T. Ensslen, H. Gottschalk, M. Saadi and A. Seyfried

# ASSESSMENT OF MODELS FOR PEDESTRIAN DYNAMICS WITH FUNCTIONAL PRINCIPAL COMPONENT ANALYSIS

January 31, 2015

http://www.math.uni-wuppertal.de

# ASSESSMENT OF MODELS FOR PEDESTRIAN DYNAMICS WITH FUNCTIONAL PRINCIPAL COMPONENT ANALYSIS

TIM ENSSLEN, HANNO GOTTSCHALK AND MOHAMED SAADI
*Department of Mathematics and Computer Science,*
*Bergische Universität Wuppertal, 42119 Wuppertal, Germany,*
{tim.ensslen,hanno.gottschalk,saadi}@uni-wuppertal.de

MOHCINE CHRAIBI AND ARMIN SEYFRIED
*Jülich Supercomputing Centre,*
*Forschungszentrum Jülich GmbH, 52428 Jülich, Germany*
*and*
*Department of Civil Engineering,*
*Bergische Universität Wuppertal,*
*Pauluskirche 7, 42285 Wuppertal, Germany*
{m.chraibi,a.seyfried}@fz-juelich.de

Many agent based simulation approaches have been proposed for pedestrian flow. As such models are applied e.g. in evacuation studies, the quality and reliability of such models is of vital interest. Pedestrian trajectories are functional data and thus functional principal component analysis is a natural tool to asses the quality of pedestrian flow models beyond average properties. In this article we conduct functional PCA for the trajectories of pedestrians passing through a bottleneck. We benchmark two agent based models of pedestrian flow against the experimental data using PCA average and stochastic features. Functional PCA proves to be an efficient tool to detect deviation between simulation and experiment and to asses quality of pedestrian models.

PACS numbers: 89.75-k Complex Systems, 50.40-a Stochastic Models
Keywords: pedestrian dynamics; statistical analysis; comparison with experiment; functional PCA; model quality

## I. INTRODUCTION

Most of the force-based models qualitatively describe the movement of pedestrians. Self-organization phenomena e.g., lane formations [5, 6, 21], oscillations at bottlenecks [5, 6], clogging at exit doors [5, 21] etc., are reproduced.

In order to produce reliable and safety relevant assertions quantitative validation of mathematical models is of tremendous importance. In most known cases this is fulfilled by reproducing the fundamental diagram [2, 8, 11, 18] or measuring the flow through bottlenecks [2, 7]. An overview of quantitative validation of models by means of the fundamental diagram is given in [16]. On one hand, the common point between these quantitative methods is the fact that they are based on calculating specific traffic quantities, e.g. density, flow and velocity. On the other hand, these measurements are performed based on locally averaged values over time or space. [22] gives a comprehensive summary of different measurement methods. ut state of the art models describe these system on a more detailed level by calculating trajectories of single pedestrians. Thus we follow a different approach. Based on the trajectories of pedestrians resulting of a simulation, we extract quantitative characteristics of the statistical ensemble of trajectories taken by the agents. Doing the same for the experiment then allows to make an assessment on the quality of the investigated model.

While there is an abundance of agent based models in the field of pedestrian or traffic dynamics, the question of systematic comparison of experimental evidence and model generated results has not caught the same attention. This would however be important for the ranking of models into more or less adequate ones. Given that many applications of pedestrian dynamics are safety relevant, the need to evaluate models with some well established methodology is evident. The methodology of the evaluation should provide a comparison of model results and empirical data corresponding to the level of detail of the model. It is desirable that such a method should not only be able to asses average pedestrian or traffic flow behaviour, but also account for the amount and typical nature of fluctuation around this average.

Among the difficulties in the field is the fact that in agent based pedestrian or traffic flow data is functional, i.e. to each individual we associate data in the infinite dimensional space of trajectories $x(t)$. The adequate statistical language for the study of pedestrian or traffic flow data is thus the well established method of functional data analysis [15]. In this field, the variation in the trajectories of different agents is interpreted as random fluctuations. Thus, the measured or simulated trajectories are interpreted as realizations of some stochastic process $X(t) \in \mathbb{R}^2$, where $t$ stands for a time parameter and $X(t) = X(t, \omega)$ tacitly depends on some random parameter $\omega$ from a probability space $(\Omega, \mathcal{A}, P)$, confer e.g. [1] for further details.

Although there are infinitely many trajectories available for an agent to move from point A to point B, it often turns out that a few typical modes of variation around the average movement are responsible for the bulk of fluctuation of trajectories between different individuals. As a classical method in the analysis of functional data, the functional principal component analysis (PCA) is the standard method to find and analyse these typical variations.

The scope of this article is to use functional PCA analysis to study the performance of agent based models of pedestrian motion with experimental data from pedestrian flow through a bottleneck as the benchmark. In order to demonstrate the methodological approach, two models – social force model (SFM) [10] and generalized centrifugal force model (GCFM) [2] – are used to simulate pedestrian trajectories in with a bottleneck of the same dimensions. In the following we apply functional PCA using the open source extension `fda` by Ramsey, Hooker and Graves [14] to the statistics language `R` to conduct the analysis. We present the results and give a detailed comparison of average values for locations and velocities and their respective principal components. For the latter we separately compare strength, distribution of total variation, and morphology of principal components.

We show that functional PCA in fact can be used to make statistically significant statements about model quality. Functional PCA reveals significant deviation between both models and experiment already on the level of average values. While the morphology of principal components for locations is more or less adequately represented by both models, there are significant deviations in the strength of fluctuations around the mean behaviour with the GCFM models underestimating the experimentally observed fluctuations while the SFM mostly overestimates fluctuation strength. These empirical observations can be confirmed with statistical testing for significance using the PCA-bootstrap methodology [3, 4].

The article is organized as follows. In Section II we review the pedestrian flow experiment [17] as the benchmark case for this study. Section III gives a brief account on the SFM and the GCFM model. In Section IV reviews the functional PCA and its numerical implementation. Section V is the main part of this article. After some introductory remarks on data formatting and smoothing (Subsection V A), we compare average data for x and y position data (Subsection V B) and velocities directed in the main direction of motion, which is the $x$-direction. We then compare fluctuations strength via PCA eigen values (Subsection V C) and morphology for the first PCA harmonics for $x$- and $y$- positions and $x$-velocities (Subsection V D). Section VI presents the PCA-bootstrap approach in the context of spline-based PCA (Subsection VI A) and applies this to total variation and Gini index (Subsection VI B) as well as the $L^2$-distance of the average trajectories and the Hilbert Schmid distance of the empirical correlation functions

(Subsection VI C). In Section VII we summarize or findings and give some conclusions on model quality in the specific case and general applicability of functional PCA in the given context.

## II. EXPERIMENT

In this work we use as a reference the experimental data extracted from the experiment [17]. that was performed in 2006 in the wardroom of the "Bergische Kaserne Düsseldorf". See Fig. 1.

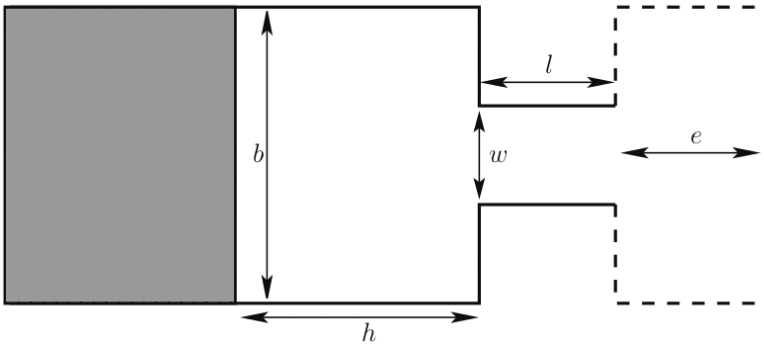


FIG. 1. The simulation set-up: pedestrians start from the shaded area and move through the bottleneck ($l = 4$ m, $h = 4.5$ m, $b = 6$ m and $w = 0.9$ m). An adjacent area of length $e = 2.5$ m is added to consider the backward effect of leaving pedestrians on those still in the bottleneck.

A waiting area was used to distribute the attendees before the start of each run of the experiment.

For simulation purposes we enlarge the area of the set-up by an extra room of length $e$. This is necessary to take into consideration the effects of pedestrians that leaved the bottleneck on the pedestrians still in the system.

The flow through the bottleneck is measured as follows:

$$J = \frac{N}{\Delta t}, \tag{1}$$

with $N$ the number of pedestrians and $\Delta t = t_{\text{last}} - t_{\text{first}}$ the time gap between the first and the last pedestrian passing the bottleneck at measurement line.

## III. MODELS

Force-based models describe the movement of pedestrians as a superposition of forces. Given the state variables of pedestrian $i$ at time $t$ $(\overrightarrow{x_i}(t), \overrightarrow{v_i}(t))$ and considering Newton's second law of dynamics the state of each pedestrian $i$ is defined by:

$$m_i \overrightarrow{a_i}(t) = \sum_{i \neq j} \overrightarrow{f_{ij}^r} + \sum_{W} \overrightarrow{f_{iw}^r} + \overrightarrow{f_i^d}, \tag{2}$$

and

$$\overrightarrow{v_i}(t) = \frac{d\overrightarrow{x_i}(t)}{dt}, \tag{3}$$

where $\overrightarrow{f_{ij}^r}$ denotes a repulsive force acting from the $j^{th}$-pedestrian on the $i^{th}$-pedestrian, $\overrightarrow{f_{iw}^r}$ is a repulsive force emerging from borders, walls etc. and $\overrightarrow{f_i^d}$ is a driven force. $m_i$ is the mass of pedestrian $i$.

The superposition of the forces reflect the fact that pedestrians move towards a certain point in space (e.g. an exit) and meanwhile try to avoid collisions with each other or with walls and objects.

The driving force $\overrightarrow{f_{ij}^r}$ models, at low densities, an exponential acceleration towards a desired speed $v_0$: The following expression [13] is used:

$$\overrightarrow{f_i^d} = m_i \frac{v_0 \overrightarrow{e_i^0} - \overrightarrow{v_i}}{\tau}, \tag{4}$$

with a relaxation time $\tau$ typically equal to 0.5 s , and a desired direction $\overrightarrow{e_i^0}$ of pedestrian $i$.

The repulsive force between pedestrians $\overrightarrow{f_{ij}^r}$ is defined differently from one model to another [2, 6, 18, 19, 21].

In this work we study a variation of the social force model (SFM) and the generalized centrifugal force model [2]. Both models are microscopic and continuous in space. In the GCFM the agents have an elliptical form with velocity-dependent semi-axes, whereas the shape of agents in the SFM is circular. In the general case, the distance $\| \overrightarrow{d_{ij}} \|$ is defined as the distance between the borders of the ellipses $i$ and $j$ along a line connecting their centres. See Fig. 2. For the SFM the semi-axis orthogonal to the movement direction is equal to the other semi-axis in the direction of movement. For simplicity we write $d_{ij}$ to denote the norm of the vector $\overrightarrow{d_{ij}}$.

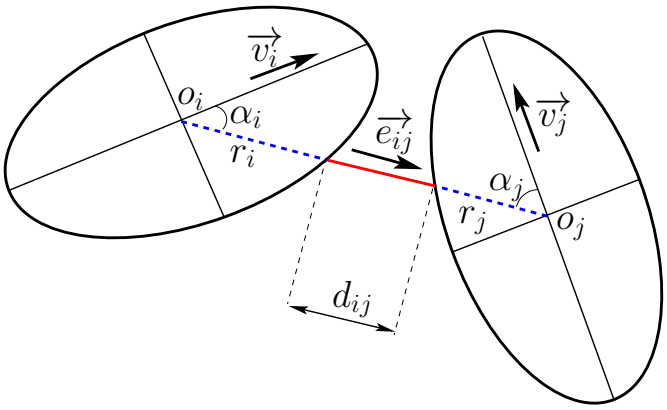


FIG. 2. The effective distance $d_{ij}$ of two pedestrians represented by two ellipses.

### A. The social force model (SFM)

The SFM as originally published by Molnár [10] describes the movement of circular agents as superposition of different factors e.g. influence of neighboring pedestrians, walls, attractions and groups. In this work we reduce the complexity of the model to a minimum, considering only the influence of pedestrians and walls and assuming only circular potentials.

The repulsive force in the SFM between agent $i$ and $j$ is defined as

$$\overrightarrow{f_{ij}^r} = -m_i k_{ij} A \exp(\frac{d_{ij}}{B}) \overrightarrow{e_{ij}}. \tag{5}$$

with

$$\overrightarrow{d_{ij}} = \| \overrightarrow{x_j} - \overrightarrow{x_i} \| - r_i - r_j, \tag{6}$$

and

$$\overrightarrow{e_{ij}} = \frac{\overrightarrow{x_j} - \overrightarrow{x_i}}{\| \overrightarrow{x_j} - \overrightarrow{x_i} \|}, \tag{7}$$

With the parameters $A$ and $B$ the strength and the range of the force are adjusted. The limited vision of pedestrians (180°) is modeled by the coefficient $k_{ij}$:

$$k_{ij} = \Theta\Big(\overrightarrow{v_i}.\overrightarrow{e_{ij}}\Big). \tag{8}$$

$\Theta(\cdot)$ is the Heaviside function. The repulsive force between pedestrians and static objects is defined similarly to (5).

### B. The generalized centrifugal force model (GCFM)

The repulsive force in the GCFM is inversely proportional to the distance of two ellipses representing moving pedestrians $i$ and $j$ and depends on their relative velocity:

$$\overrightarrow{f_{ij}^{r}} = -m_i \frac{\Big(\alpha v_0 + v_{ij}\Big)^2}{d_{ij}}, \tag{9}$$

where $v_{ij} = \Theta\Big((\overrightarrow{v_i} - \overrightarrow{v_j}) \cdot \overrightarrow{e_{ij}}\Big)$, is the relative velocity. The use of the Heaviside function $\Theta(\cdot)$ ensures, that faster pedestrians are not effected by slower pedestrians. By means of the parameter $\alpha$ the strength of the force can be adjusted. As mentioned earlier in the GCFM the space requirement in the direction of movement is modeled by the semi-axis

$$a = a_{\min} + \tau_a v_i, \tag{10}$$

with two parameters $a_{\min}$ and $\tau_a$, whereas the lateral swaying of pedestrians is modeled by the semi-axis

$$b = b_{\max} - (b_{\max} - b_{\min})\frac{v_i}{v_0}. \tag{11}$$

### C. Model parameters

As mentioned earlier the original SFM includes several forces e.g. physical contact forces and attractive forces. For our purpose we use a simplified version of the SFM as presented in Sec. III A. We choose $A = 5$ N for pedestrian-pedestrian interactions (5) and $A = 7$ N for pedestrian-wall interactions. The range of the function defined by the parameter $B$ in (5) was chosen to be 0.08 m for pedestrian-pedestrian interactions and 0.05 m for pedestrian-wall interactions. The parameter $\alpha$ in (9) is set to 0.2 for pedestrian-pedestrian interactions and 0.33 for pedestrian-wall interactions. The desired speed $v_0$ is set to $\mu = 1.1$ m/s. For simplicity we set for both models $m_i = 1$ Kg. Table I gives a resume of the parameters used.

| Parameter | Equation | Value |
|---|---|---|
| $A_{\text{ped}}$ | (5) | 5 N |
| $A_{\text{wall}}$ | Similar to (5) | 7 N |
| $B_{\text{ped}}$ | (5) | 0.08 m |
| $B_{\text{wall}}$ | Similar to (5) | 0.05 m |
| $\alpha_{\text{ped}}$ | (9) | 0.2 |
| $\alpha_{\text{wall}}$ | Similar to (9) | 0.33 |
| $\tau$ | (4) | 0.5 s |
| $v_0$ | (4) | 1.1 m/s |
| $m$ | (4) | 1 Kg |
| $a_\tau$ | (10) | 0.12 s |
| $a_{\min}$ | (10) | 0.15 m |
| $b_{\min}$ | (11) | 0.15 m |
| $b_{\max}$ | (11) | 0.2 m |

TABLE I. Parameter values in simulations with both GCFM and SFM.

The values chosen in Tab. I differ from the values published in other works [2, 9]. Our choice of the above mentioned values is supported by qualitative reasons, ensuring minimal overlapping among pedestrians, as well by quantitative consideration of the flow through the bottleneck. See Fig. 3.

For safety relevant simulations a careful calibration of the used models is needed. In this paper we strive to apply a new technique to assert the goodness of pedestrian dynamics models.

## IV. FUNCTIONAL PCA: FOUNDATIONS

### A. What is functional PCA?

In this section we give some details of functional PCA following [15]. The principle component analysis uses the principle axis transformation for multivariate, correlated numerical data using the (empirical) covariance information

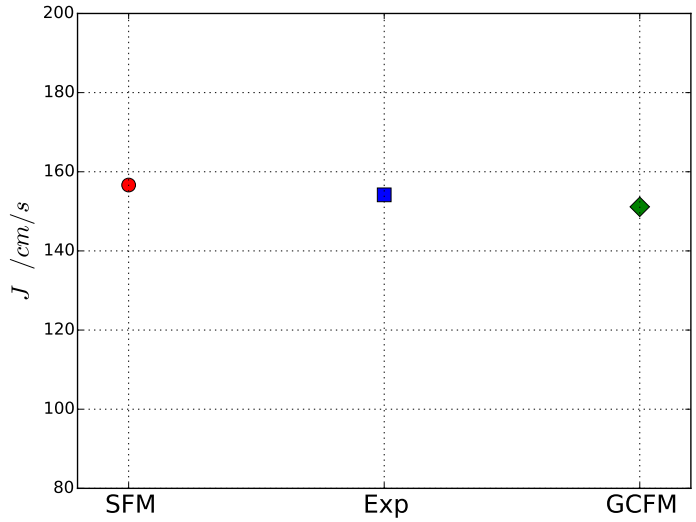


FIG. 3. The flow through the bottleneck measured at the middle of the corridor after the entrance to the bottleneck. The empirical value is a reference value for the calibration of the GCFM and the SFM.

between the single random variables. This is by means of the eigen function decomposition of the empirical covariance matrix. Eigen values then sort the importance of the single eigen vectors (also called harmonics or modes) according to the variance. In the next step the data can be projected in a low dimensional subspace without significant loss of information, provided that only a few eigen values are significantly different from zero.

The result of the PCA is a subspace – spanned by a few eigen vectors of the covariance matrix – which describes the data with fewer dimension and hardly any loss of information about the variance of the data. This concept needs to be adapted to the case where the observed data from $n$ individuals are functions – as it is the case with the trajectories of pedestrians. The variability of the data can still be described in with the eigenvalues and eigenvectors of the covariance function seen as an operator on the function space of square integrable functions. Given the stochastic process of random trajectories $X(t)$, with $t \in (0, L)$, the covariance function is defined as

$$C(s,t) = \mathbb{E}\left[(X(s) - \mathbb{E}[X(s)])(X(t) - \mathbb{E}[X(t)])\right], \tag{12}$$

with $\mathbb{E}$ the expected value with respect to the underlying probability space. This covariance function needs to be estimated out of the data $x_j(t)$

$$\hat{C}(s,t) = \frac{1}{n-1}\sum_{j=1}^{n}(x_j(s) - \bar{x}(s))(x_j(t) - \bar{x}(t)), \tag{13}$$

with $x_j(t)$ the $j$-th observation is one realization of the random process $X(t)$ and $\bar{x}(t) = \frac{1}{n}\sum_{j=1}^{n} x_j(t)$.

In the following we assume that average values have all ready been removed from the stochastic signal, i.e. we consider transformed random quantities $X(t) \to X(t) - \mathbb{E}[X(t)]$ with estimated observations $x_i(t) - \bar{x}(t)$. The eigenvalues of $C(s,t)$ can then be calculated after solving the follow eigen value equation

$$\int_0^L C(s,t)\xi(t)\,dt = \lambda\,\xi(s). \tag{14}$$

This results in a set of eigen values $\lambda_1 \geq \lambda_2 \geq \cdots \geq 0$ and corresponding eigen functions $\xi_i(s)$. These eigen functions are orthonormal $\int_0^L \xi_i(t)\xi_j(t)\,dt = \delta_{i,j}$, where $\delta_{i,j} = 1$ for $i = j$ and zero otherwise. The eigen functions and eigen values can now approximately be determined from the observations $x_j(t)$ by replacing $C(s,t)$ by its empirical counterpart $\hat{C}(s,t)$.

### B. Numerical approximation

The problem (14) is an infinite dimensional eigen value problem and its empirical counter part is potentially very high dimensional (of dimension $n$). A frequently used method to make this problem numerically tractable is to project the covariance matrix on the space spanned by some finite basis, - e.g. a sufficiently fine B-spline or Fourier basis. Then one solves for the eigen values and functions in the given finite dimensional space of basis functions. Therefore we approximate the observed functions $x_i(t)$ with a suitable linear combination of basis functions

$$x_i(t) \approx \sum_{k=1}^{K} c_{i,k}\Phi_k(t) \Leftrightarrow x_i(t) \approx \mathbf{C}\mathbf{\Phi}(\mathbf{t}), \tag{15}$$

with basis function vector $\Phi(t) = (\Phi_1(t), \ldots, \Phi_K(t))^T$ and coefficient matrix $\mathbf{C} = (c_{j,k})_{\substack{j=1,\ldots,n \\ k=1,\ldots,K}}$ obtained e.g. by orthogonal projection of $x_i(t)$ to the space spanned by the basis functions and a subsequent basis decomposition, in which case $\mathbf{C} = \mathbf{W}^{-1}\mathbf{v}_j$ with $W_{i,j} = \langle \Phi_i, \Phi_j \rangle = \int_0^L \Phi_i(t)\Phi_j(t)\,ds$ and $c_{j,k} = \langle x_j, \Phi_k \rangle = \int_0^L x_j(t)\Phi_k(t)\,dt$. Here some numerical quadrature may be employed for the integrals involved in the definition of $v_{j,k}$, whereas in most cases analytic formulae are available for $W_{i,j}$. This projection method implies that the covariance function can be approximated by

$$\hat{C}(s,t) \approx \frac{1}{n-1}\Phi(s)^T\mathbf{C}^T\mathbf{C}\Phi(t). \tag{16}$$

Now we expand the eigen function with the same basis functions to a good approximation:

$$\xi(t) \approx \sum_{k=1}^{K} b_k\Phi_k(t) = \Phi(t)^T\mathbf{b}. \tag{17}$$

The approximate eigen value equation can be written as

$$\begin{aligned} \int_0^L \hat{C}(s,t)\xi(t)\,dt &\approx \int_0^L \frac{1}{n}\Phi(s)^T\mathbf{C}^T\mathbf{C}\Phi(t)\Phi(t)^T\mathbf{b}dt \\ &= \frac{1}{n}\Phi(s)^T\mathbf{C}^T\mathbf{C}\mathbf{W}\mathbf{b} \\ &= \lambda\Phi(s)^T\mathbf{b} \approx \lambda\xi(s). \end{aligned} \tag{18}$$

leading to the eigen value equation

$$\mathbf{C}^T\mathbf{C}\mathbf{W}\mathbf{b} = \lambda\mathbf{b} \Leftrightarrow \mathbf{W}^{1/2}\mathbf{C}^T\mathbf{C}\mathbf{W}^{1/2}\mathbf{u} = \lambda\mathbf{u},\ \mathbf{b} = \mathbf{W}^{-1/2}\mathbf{u}, \tag{19}$$

which can be solved numerically. The result is a number of eigen values $\lambda_1 \geq \lambda_2 \geq \cdots \geq 0$ and coefficient vectors $\mathbf{b}_i$ for approximate principal components $\xi_i(t) = \Phi(t)^T\mathbf{b}_i$, $i = 1, 2, \ldots$.

### C. Statistics of the eigen values

In this subsection, we discuss how to reduce the information from the set of eigen values to a few significant characteristics. In particular we will focus on code figures that measure the strength of fluctuations and their concentration to a few, active modes.

The eigen value $\lambda_i$ represents the strength of fluctuations in the respective mode of characteristic shape $\xi_i(t)$. The relative strength $\rho_i$ of the variation in the mode $\xi_i(t)$ and the cumulative relative strength $L_j$ up to the $j$-th mode $\xi_j(t)$ is given by

$$\rho_i = \frac{\lambda_i}{\sum_{j=1}^n \lambda_j} \text{ and } L_j = \sum_{i=1}^{j} \rho_i. \tag{20}$$

Two quantities that can be derived form the eigen values of the PCA are of special interest: First, the total variation strength is simply the sum of all eigen values $\Lambda = \sum_{j=1}^n \lambda_j$ whereas the Gini index is a measure of concentration that is build from the Lorenz curve quantities $L_j$ via $G = \frac{2}{n-1}\sum_{j=1}^n (L_j - j/n)$. Geometrically, the Gini index measures

the area between the diagonal and the Lorentz curve, cf. e.g. Figure 9 in the right panel. It is normalised such that it takes the value one if only one mode is active and takes the value zero when all modes are equally activated $\lambda_1 = \lambda_2 = \cdots = \lambda_n$. Note that the order of $\lambda_j$ is descending in contrast to the usual definition of the Gini index, where the order is ascending.

As an alternative, one could also consider the entropy of the distribution of the total activity to the single modes. The result of the observation however remain largely unchanged.

### D. Deviation measures

In this section we derive some quantities that can be used to measure the distance between one set of functional data and another such data set. In particular we will utilize these distances for benchmarking models with respect to their distance to the experiment. Two distance measures will be employed in the following: First, the mean quadratic deviation between the average trajectories of the model on the one hand and the experimental data on the other. Secondly, we consider the Hilbert-Schmidt norm between the respective empirical covariance functions as a measure of the distance of the fluctuation behaviour of the experiment and the simulation. In the following we work with the data after projection to a finite spline basis $\Phi_k(t)$.

We start with the mean quadratic difference in the average behaviour. The mean of the observed function $x_i(t)$ is :

$$\overline{x}(t) = \frac{1}{n}\sum_{j=1}^{n} x_j(t) = \sum_{k=1}^{K}\Bigg(\overbrace{\frac{1}{n}\sum_{j=1}^{n} c_{jk}}^{=C_k}\Bigg)\Phi_k(t) = \sum_{k=1}^{K} C_k\Phi_k(t). \tag{21}$$

We can write the $L^2$ norm of $\overline{x}(t) = \sum_{k=1}^{K} C_k\Phi_k(t)$ in matrix form as:

$$||\overline{x}(t)||_2^2 = \left\langle \sum_{k=1}^{K} C_k\Phi_k(t), \sum_{k=1}^{K} C_k\Phi_k(t) \right\rangle = \mathbf{C}^T\mathbf{W}\mathbf{C}. \tag{22}$$

The mean quadratic distance, the squared $L^2$ norm, of the difference between $\overline{x}(t) = \sum_{k=1}^{K} C_k\Phi_k(t)$ and $\overline{y}(t) = \sum_{k=1}^{K} C_k^{'}\Phi_k(t)$ is:

$$\begin{aligned}\|\overline{x}(t) - \overline{y}(t)\|_2^2 &= \int_0^L (\overline{x}(t) - \overline{y}(t))^2 dt \\ &= \left\langle \sum_{k=1}^{K}(C_k - C_k^{'})\Phi_k(t), \sum_{k=1}^{K}(C_k - C_k^{'})\Phi_k(t) \right\rangle \\ &= (\mathbf{C} - \mathbf{C}')^T\mathbf{W}(\mathbf{C} - \mathbf{C}').\end{aligned} \tag{23}$$

We now derive formulae for measuring the distance between experiment and simulation in the covariance structure. For the empirical covariance function $\hat{C}(s,t)$, we can write

$$\begin{aligned}\hat{C}(s,t) &= \frac{1}{n-1}\sum_{j=1}^{n}(x_j(s) - \bar{x}(s))(x_j(t) - \bar{x}(t)) \\ &= \frac{1}{n-1}\sum_{j=1}^{n}\Bigg(\sum_{k=1}^{K} c_{jk}\Phi_k(t) - \sum_{k=1}^{K} C_k\Phi_k(t)\Bigg)\Bigg(\sum_{l=1}^{K} c_{jl}^{'}\Phi_l(s) - \sum_{l=1}^{K} C_l^{'}\Phi_l(s)\Bigg) \\ &= \sum_{k=1}^{K}\sum_{l=1}^{K}\underbrace{\Bigg(\frac{1}{n-1}\sum_{j=1}^{n}\big(c_{jk} - C_k\big)\big(c_{jl}^{'} - C_l^{'}\big)\Bigg)}_{=\mathbb{C}_{k,l}}\Phi_k(t)\Phi_l(s) \\ &= \sum_{k=1}^{K}\sum_{l=1}^{K}\mathbb{C}_{k,l}\Phi_k(t)\Phi_l(s).\end{aligned} \tag{24}$$

Let $\hat{D}(s,t) = \hat{C}(s,t) - \hat{C}'(s,t) = \sum_{k=1}^{K}\sum_{l=1}^{K}(\overbrace{\mathbb{C}_{k,l} - \mathbb{C}'_{k,l}}^{=\mathbb{D}_{k,l}})\Phi_k(t)\Phi_l(s)$ be the difference of covariance functions. The Hilbert-Schmidt norm of $\hat{D}(s,t)$ is :

$$\begin{aligned}\|\hat{D}\|_{HS}^2 &= \int_0^L \int_0^L \left(\hat{D}(s,t)\right)^2 dsdt \\ &= \sum_{k=1}^{K}\sum_{l=1}^{K}\sum_{k'=1}^{K}\sum_{l'=1}^{K} \int_0^L \Phi_k(t)\Phi_{k'}(t)dt \int_0^L \Phi_l(s)\Phi_{l'}(s)ds\mathbb{D}_{kl}\mathbb{D}_{k'l'} \qquad (25)\\ &= \sum_{k=1}^{K}\sum_{l=1}^{K}\sum_{k'=1}^{K}\sum_{l'=1}^{K} W_{kk'}W_{ll'}\mathbb{D}_{kl}\mathbb{D}_{k'l'} = \mathrm{Tr}\big((\mathbb{D}\mathbf{W})^T\mathbb{D}\mathbf{W}\big). \qquad (26)\end{aligned}$$

Here $\mathrm{Tr}(A)$ stands for the trace of the matrix $A$.

## V. PCA RESULTS

In this section we show that functional PCA is a useful tool for detailed validation of models for pedestrian dynamics. Ideally, the variability in the data can be described with the help of the PCA with a few principal components. These main components can be interpreted as the schemes for the deviation of individual trajectories from the mean flow. This allows a comparison of simulated and experimental data beyond averaged flow features. Therefore, we apply the PCA to the experimental data and simulated data from two models SFM and GCFM and compare the results. Here we do the PCA for $x$ and $y$ coordinates over time separately, as this approach is somewhat more accessible to the interpretation. We also analyse the velocity of the pedestrian in the same way. For the alternative approach of jointly analysing $x$ and $y$ trajectories and a discussion of the pros and cons of both approaches, see [14, 15].

The analysis of the data is based on the `R` package `fda` of J.O. Ramsay, Giles Hooker und Spencer Graves [14] with some minor extensions by the authors.

### A. Preparation of the Data

The pedestrian trajectory data in the experiment is recorded electronically with video tracking at the rate of 25 frames/ s. A total number of 149 trajectories has been recorded. Likewise, the SFM and GCFM models have been simulated with 25 time steps per second using Euler integration with a time step $\Delta t = 0.01$ s. For both models, a total of 149 trajectories have been simulated.

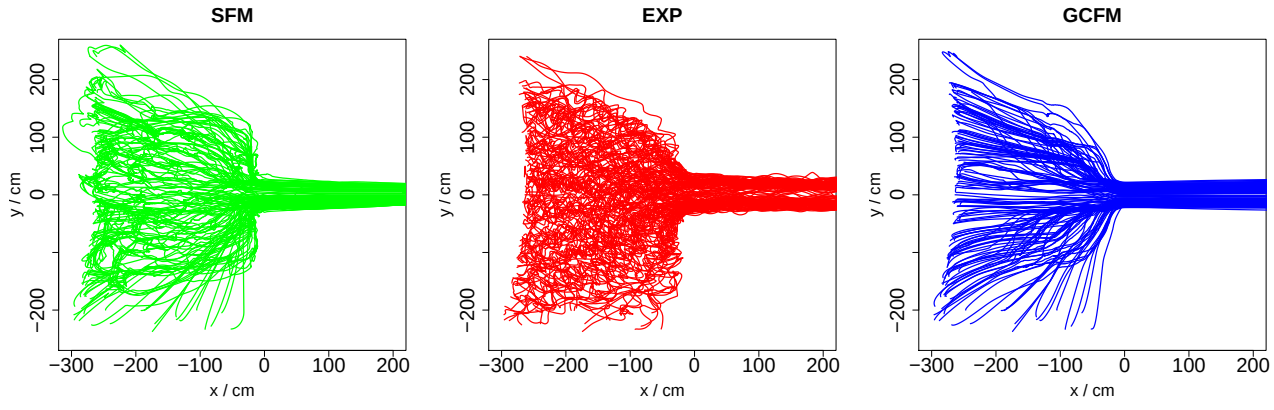


FIG. 4. XY plots of pedestrian trajectories generated by the SFM model (left), experiment (middle) and GCFM model (right).

For the analysis, the pedestrian motion has to be stationary, i.e. all agents move under the same conditions. Furthermore, the considered time interval has to be the same for all agents. Therefore we account only to the pedestrians, who need more than 12 seconds to reach the exit. Furthermore, the trajectory is tracked only two

seconds after the passage of the bottleneck entrance. The analysis of the experimental data and the models thus is based on trajectories in individual time intervals that range from $-12\,\mathrm{s}$ before passage through the bottleneck by the individual to $+2\,\mathrm{s}$ afterwards. This makes a total time of $14\,\mathrm{s}$. In order to avoid negative time values, we start each pedestrian trajectory at time $t = 0\,\mathrm{s}$ such that passage through the door for each individual occurs at $t = 12\,\mathrm{s}$, exactly. From now on we work with this time scale. Figure 5 visualizes the formatting steps. After reformatting, a total of 118 pedestrian trajectories were available for the experiment, 121 for the SFM and also 121 for the GCFM model, respectively.

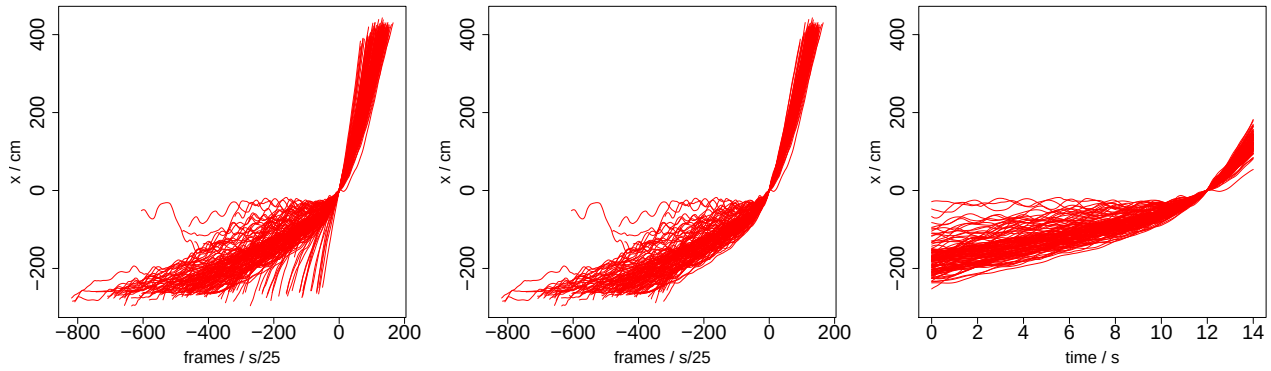


FIG. 5. Plots of $x$-coordinates of pedestrians (experimental data): raw data (left), stationary data (middle) and with individual time in the interval [0,14] s (right). One Frame in the first two panels corresponds to 1/25 s.

The experimental data contain the swaying caused by the bipedal locomotion of pedestrians in combination with the tracking of markers on the had. But the SFM as well as the GCFM model the movement of the centre of mass neglecting the bipedal locomotion. Therefore, we smooth the data before the analysis in order to filter out swaying. It turns out that the regression with a B-spline basis containing 10 elements with nodes equally distributed over the underlying time interval $[0, 14]$ effectively removes swaying while properly reproducing the other features of the individual's trajectories, see Figure 6.

### B. Average trajectories

As PCA components describe variation around some mean, it is essential to analyse average functions $\bar{x}(t)$, $\bar{y}(t)$ and $\bar{v}_x(t)$ first. Here and in the following we leave out the analysis of the velocity component $v_y(t)$, as it presumably is of minor importance in pedestrian flow through a bottleneck with an opening along the $y$-axis.

Figure 7 shows the mean functions $\bar{x}(t)$ and $\bar{y}(t)$ of the $x$- and $y$-components for the experiment and the models.

When we look at the $x$-component, we see clear distinctions between the experiment and both models. The average pedestrian in the experiment shows a nearly linear progress to reach the exit. The acceleration after passing the bottleneck, i.e. the increase in the slope, is modest. In contrast, both SFM and GCFM show a slower progress of the average pedestrian through the crowd and a much more pronounced acceleration after the passage of the bottleneck. While the latter deviation from experiment is about the same for both models, the under estimation in the slope from the experimentally observed value is bigger for the GCFM model. Thus both models overestimate the dwell time indicating a missing anticipation and cooperation of the modelled pedestrians. However the SFM produces this effect to by a lesser amount.

The $y$-component is described by both models in a satisfactory manner, as trend lines only move at a scale of a few centimeters from the center of the bottleneck. At least for the simulated data this is due to the left hand - right hand reflection symmetry of the agents in both models and the (approximate) symmetry of initial positions with respect to the $y = 0$ axis, i.e. the center line through the bottleneck. In the experiment, a certain asymmetric behaviour is visible for the mean $y$-position of the trajectories over time. In average, the pedestrians approach the bottleneck coming slightly from the left seen from the direction of progress. Interestingly, this asymmetry can not be traced back to the initial conditions, as these are the same for the experimental and the simulated trajectories.

This behaviour is absent in both models, which have left-right symmetries in their respective constituting equations.

Figure 8 shows the mean curve of the x and y - velocities of the data. While the $y$-velocities in the experiment show oscillation patterns due to swaying effects, these fluctuations are much less in both models with a remarkable

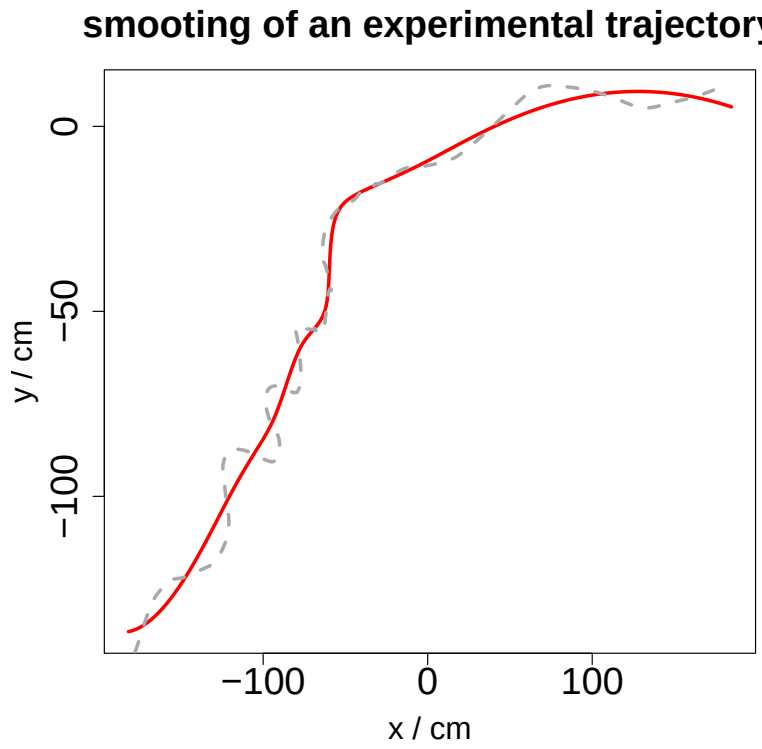


FIG. 6. Smoothing of a experimental trajectory (dotted blue) with a B-spline basis of dimension 10 (solid red).

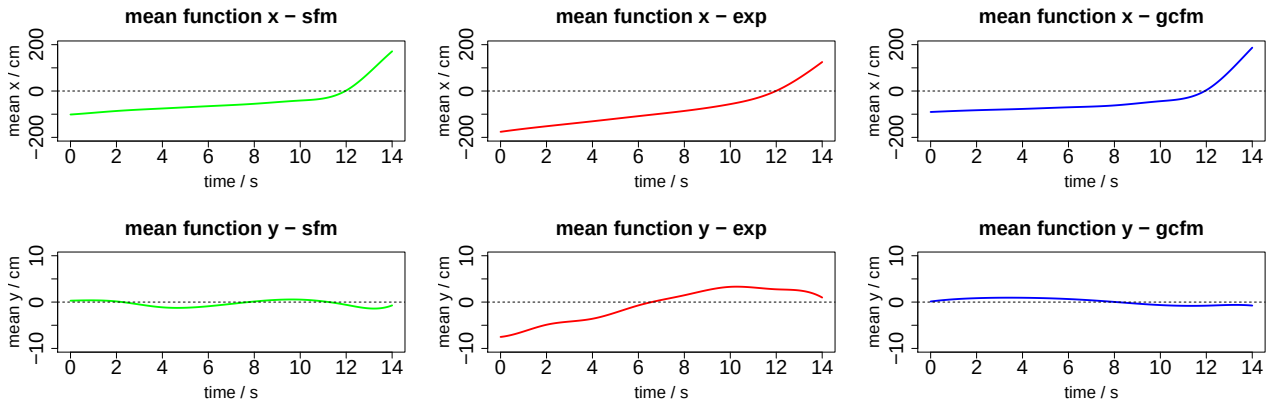


FIG. 7. Average curves for position vs time for the SFM (left), experiment (middle) and GCFM (right): $x$-ccordinate (top) and $y$-coordinate (right).

regularity in the GCFM model. As the $y$-velocities do not contribute much to the dwell time, the analysis of these data is not pursued further.

The average $x$-velocities confirm the qualitative analysis of the average $x$-positions over time. Quantitatively, the pedestrian's average speed in the exit part after 12s of time is overestimated by both models by approximately a factor of two. In both models, the average acceleration happens on a much smaller time scale as compared with experiment. As already seen, model mean velocities before the bottleneck underestimate the average experimental velocity and overestimate it after passage.

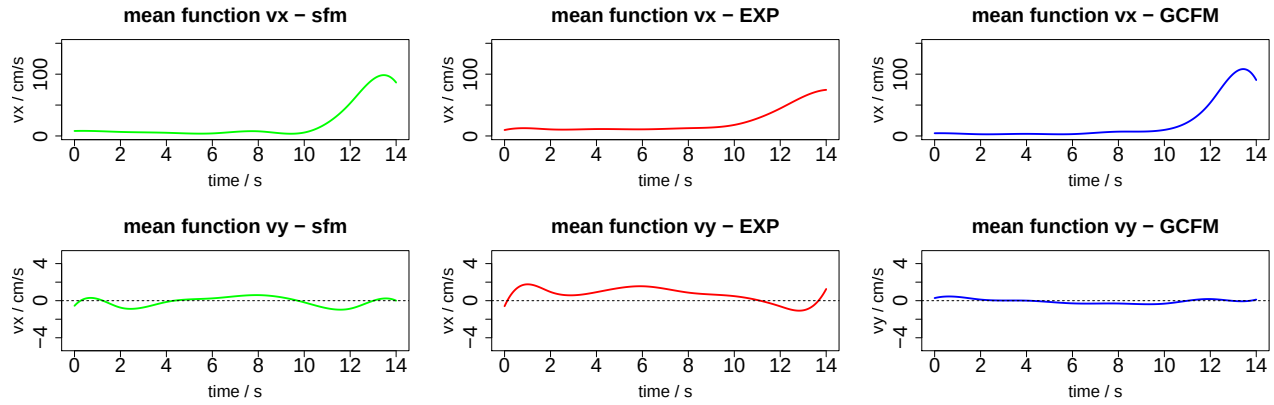


FIG. 8. Velocities over time averaged over all individuals in $x$-direction (red) and $y$-direction (blue) for the SFM model (left), the experimental data (middle) and the GCFM model (right).

### C. PCA eigen values

Having analysed the average behaviour, we now turn to the question, how well the models describe fluctuations in pedestrian data around the averages. We start with the absolute strength of PCA variability, which is represented by the PCA eigen values $\lambda_i$, $i = 1, \ldots, 10$, as we are using a 10 dimensional spline basis. At the same time, we also consider the cumulative relative strength $\varrho_j$ in order to measure the concentration or dispersion of variability in experimental or the simulated data.

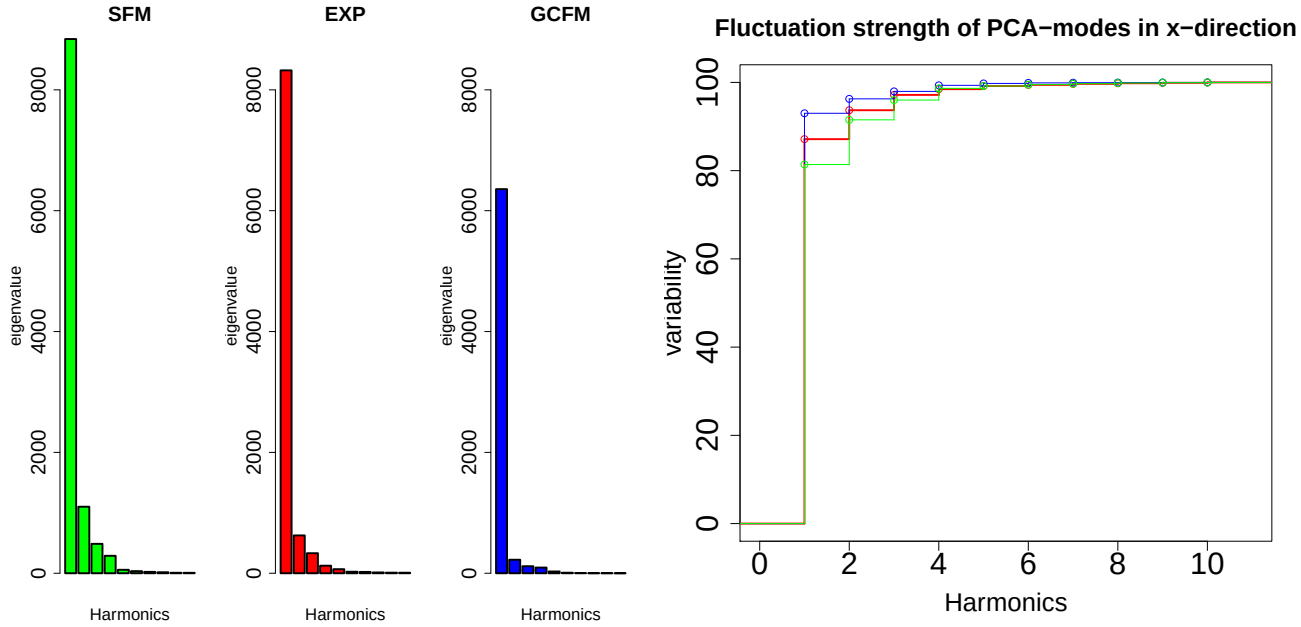


FIG. 9. Left: Barplot of absolute fluctuation strength (eigen values) of the 10 PCA-modes (harmonics) for $x$-position over time for the SFM-model, Experiment and GCFM-model. Right: Cumulative relative strength of PCA-modes over all 10 harmonics.

We first consider PCA mode strength for $x$-position over time as given in Figure 9. These modes describe typical patterns of pedestrians lagging behind and being in front of the trajectory of the average pedestrian. The SFM overestimates the total amount of statistical deviation in $x$-position from the average $x$-position by approximately 12% as compared with the experiment. Also, concentration of variability in the first mode is slightly lower than in the experiment. In the GCFM, the total level of $x$-position variation is underestimated by 37% of the total variation.

The relative concentration in the fist mode is higher as in the experimental data by an amount comparable to the SFM, but in the opposite direction. For the values of total variation and Gini indices confer Table II.

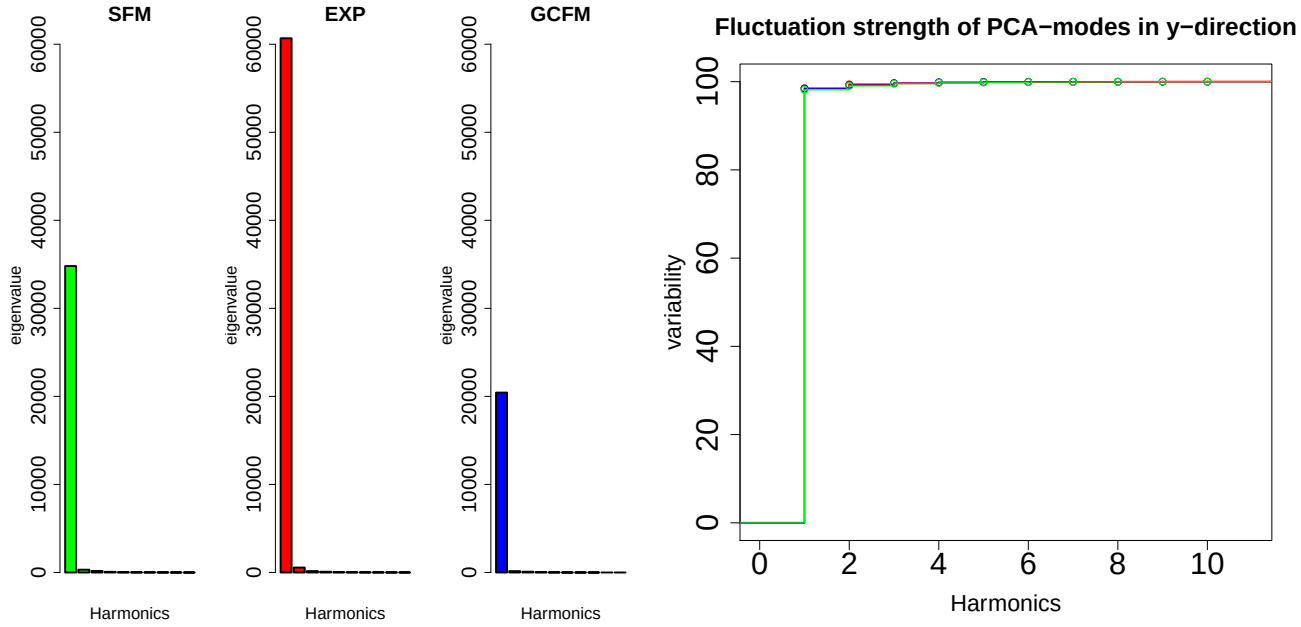


FIG. 10. Left: Barplot of absolute fluctuation strength (eigen values) of the 10 PCA-modes (harmonics) for $y$-position over time for the SFM-model, Experiment and GCFM-model. Right: Cumulative relative strength of PCA-modes over all 10 harmonics.

In Figure 10 the PCA-modes for the statistical $y$-fluctuation around the average $y$-position (essentially $y = 0$) is displayed. The experiment and both simulations all show that basically only one mode is active representing the axisymmetric shape of the jammed area in front of the bottleneck. The size of this area is under estimated by both models. The GCFM predicts a pronouncedly reduced area in the $y$-direction covered by trajectories passing the bottleneck in the next 12 seconds, showing a total $y$-variation of app. 1/3 (33.6%) of the experimental data. The same figure of underestimation of $y$-variation for the SFM compared with experiment is 57%. Total variations and Gini indices can again be found in Table II.

Figure 11 represents relative and absolute strength of $x$-velocity fluctuations of individual pedestrians or agents around the average velocity $\bar{v}_x(t)$. As in the case of $x$-positions over time, the total level of SFM fluctuations over estimates the experimental value by roughly one third. This finding comes with a slightly too high concentration of variability. For the GCFM, the under estimation of $x$-velocity is much more significant, when comparing with experiment. The dispersion behaviour more far from the experiment than in the SFM case, cf. Table II, again.

Concluding this section, we would like to interpret the findings of the mode strength of the PCA. First, due to the significant under estimation of the average velocities of the pedestrians by both models, the extension of the area covered by the trajectories 12 second before and 2 seconds after the passage of the door is considerably reduced in both models, but for the GCFM in particular, when compared to the experiment, confer Fig. 12. In addition, the low values for $y$-position fluctuations points towards an effect, that GCFM-agents essentially flow through the door in frontal direction and slipping through from the side is suppressed. Whether these findings are merely calibration issues or depend on the structural properties of both models has to be left open for the moment.

| **Tot.Var** | SFM | Experiment | GCFM |
|---|---|---|---|
| $x$-position | 10863 | 9550 | 6835 |
| $y$-position | 35469 | 61619 | 20749 |
| $x$-velocities | 1371 | 923 | 447 |

| **Gini** | SFM | Experiment | GCFM |
|---|---|---|---|
| $x$-position | 0.83 | 0.85 | 0.87 |
| $y$-position | 0.89 | 0.89 | 0.89 |
| $x$-velocities | 0.55 | 0.40 | 0.60 |

TABLE II. Total variation (left) and Gini indices (right) for the eigen values of the PCA.

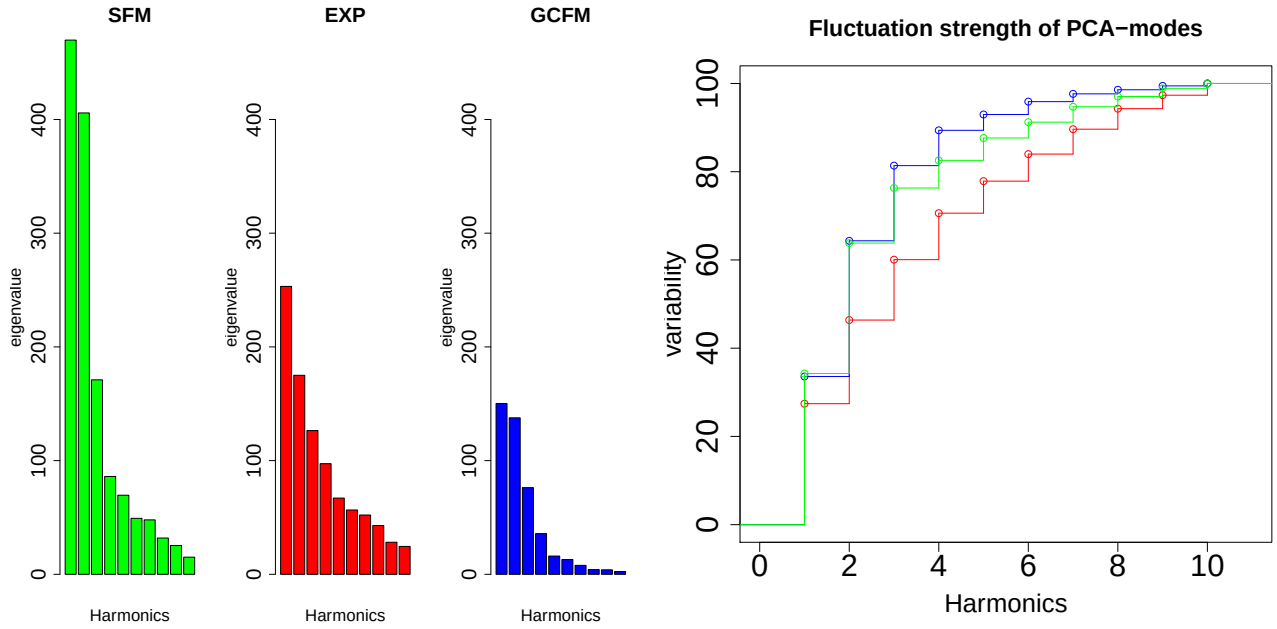


FIG. 11. Left: Barplot of absolute fluctuation strength (eigen values) of all 10 PCA-modes (harmonics) for $x$-velocity over time for the SFM-model, Experiment and GCFM-model. Right: Cumulative relative strength of PCA-modes.

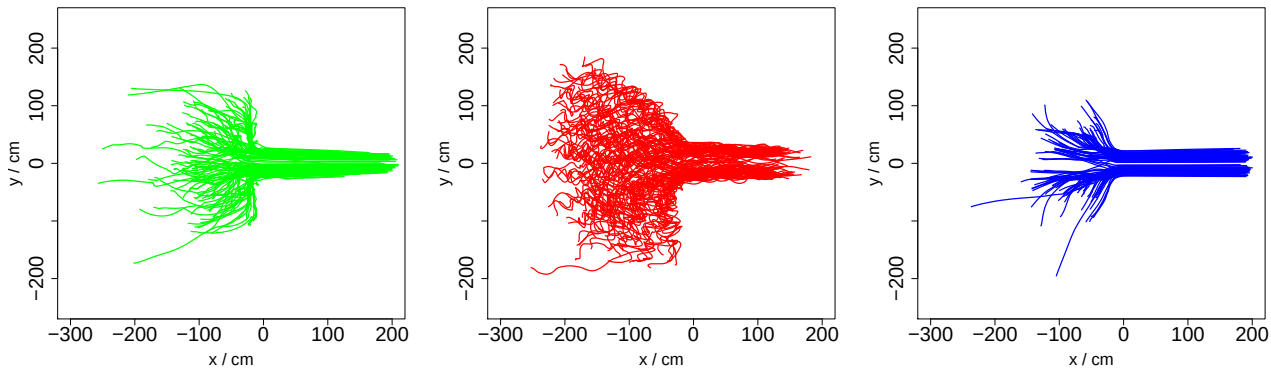


FIG. 12. Left: Trajectories of the SFM (left) Experiment (middle) and GCFM model from 12 s before to 2s after the passage through the bottleneck.

### D. PCA modes

Figure 13 shows the principal fluctuation components of the $x$-position for the experiment and the models. From the eigen value analysis above (confer Figure 9) we have seen that fluctuations can be mainly described by the first three principle components.

Let us now give an interpretation to the morphology of the PCA components. The first principle component describes the tolerance between the initial positions of the pedestrians 12 seconds before passing the bottleneck. Two pedestrians reach the bottleneck at the same reference time $t = 12$. Due to the fact that some pedestrian starts with a higher or lower $x$-distance to the bottleneck than the the others, at $t = 0$, a statistical variation in $x$-positions occurs. This could be called 'slipping through effect' because the faster pedestrian finds more favourable configurations of fellow pedestrians ahead which allows a faster passage through the crowd.

The second and third principle component describe an effect which we can associate to long stop and go behaviour in different lanes in a traffic jam: One trajectory is temporary faster than the other, but afterwards it is the other

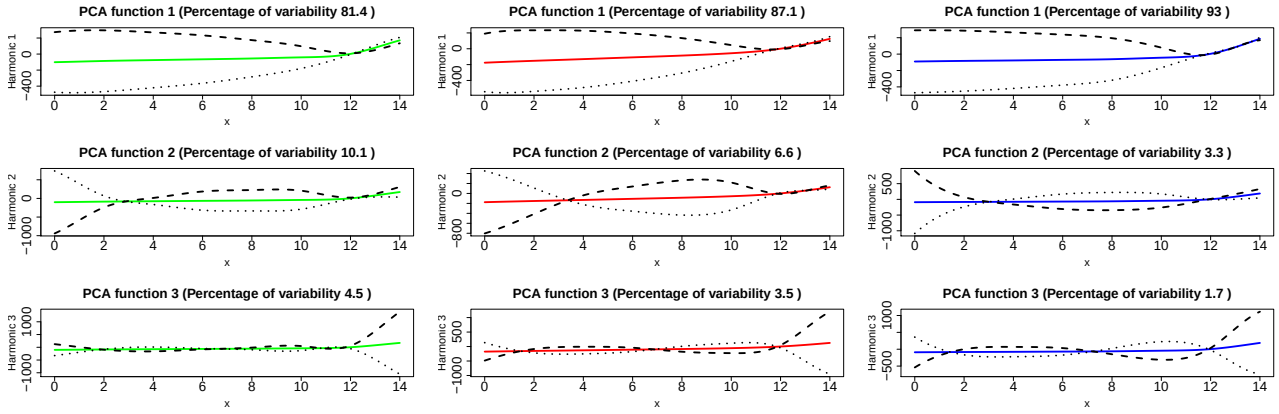


FIG. 13. PCA components in for $x$-position over time (in s/100) for the SFM model (left), experiment (middle) and GCFM model (right). The first three harmonics are displayed.

way round. In the case of the experiment and the GCFM, the third principal component also shows different velocity patterns after the bottleneck.

The morphological comparison of the experimental data with the SFM and GCFM shows that the points of intersection of the first two principal components are nearly at the same times. Thus both models reproduce the qualitative behaviour of statistical fluctuations in the pedestrians $x$-positions over time quite well. The main difference thus lies in the different activation strength of the 'slipping through' mode.

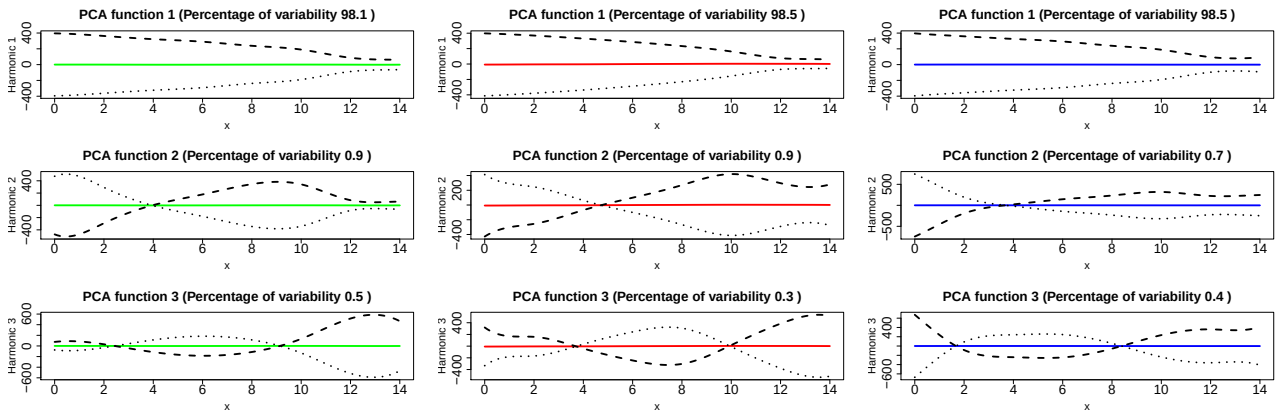


FIG. 14. PCA components in the y direction for the SFM model (left), experiment (middle) and GCFM model (right). The first three harmonics are displayed.

Figure 14 shows the PCA of the $y$-components for the experiment and the models. We can see that the variability of the data can be mainly described by the first principal component which represents the shape of the crowd in front of the door. The first principal component of both models describe the experiential data acceptably well. Also the higher modes are of quite similar shape, although one should not pay too much attention to this as these modes hardly contribute to the total variation.

We finally consider the analysis of the PCA modes for the $x$-velocity component of the pedestrians given in Fig. 15. In case of the velocity, the PCA looses the feature to project the data in a subspace of low dimension without significant loss of information. The variability of the data can only be described by a large number of components. In consequence we cannot get as much information from the analysis of a few harmonic functions, as in the two previous cases. In Figure 11 we can see the that the experimental data can be mainly described by the first seven principal components. For simplicity, we nevertheless restrict to the discussion first three components.

The morphological difference between experimental and simulated principal $x$-velocity-components is quite significant for both models when considered on the level of single components. In both models, the bulk in the variation of the $x$-velocity is occurring in the initial phase after $t = 0$ and shortly before the passage of the bottleneck, while

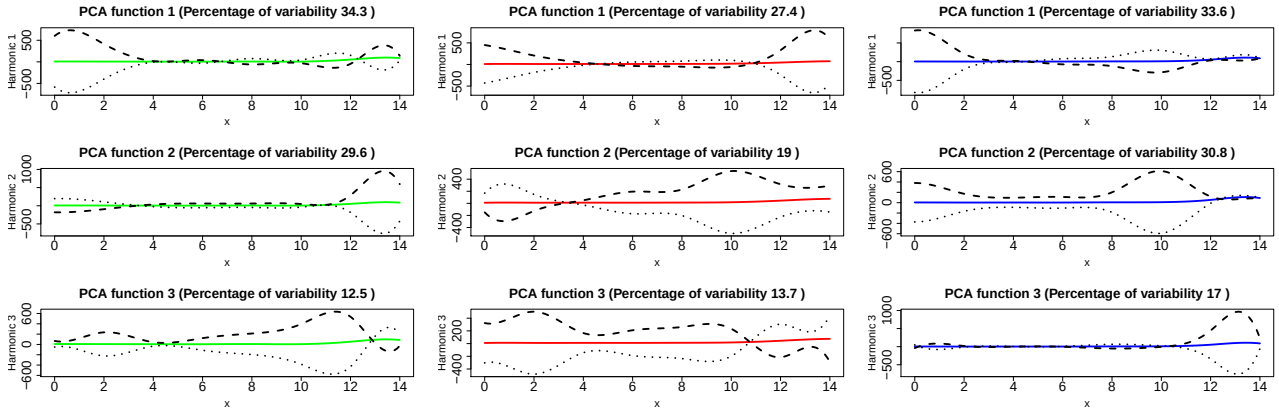


FIG. 15. PCA components of the $x$-velocity $v_x(t)$ for the SFM model (left), experiment (middle) and GCFM model (right). The first three harmonics are displayed.

for the experiment the variation in the initial phase is less and there is a pronounced variation in speed between the individuals after passing the bottle neck. The latter pattern can however be re-found in the principal component 2 of the GCFM and the principal component 3 of the CFM.

### E. Evaluation of deviation measures

Lastly in this section, we want to compare the deviation measures of the respective simulation model with the experiment. The results are summarised in III.

| $L^2$-norm | EXP-GCFM | EXP-SFM |
|---|---|---|
| $x$-position | 169.8 | 166.0 |
| $y$-position | 15.34 | 13.20 |
| $x$-velocities | 49.54 | 40.08 |

| HS-norm | EXP-GCFM | EXP-SFM |
|---|---|---|
| $x$-position | 2291 | 1282 |
| $y$-position | 4449 | 2880 |
| $x$-velocities | 286.3 | 515.1 |

TABLE III. Deviations between experimental data and models data using the $L^2$-norm (left) Hilbert-Schmidt norm (right).

In the average behaviour of $x$- and $y$- coordinates and the $x$-coordinate of the velocity of the trajectories over time in the models, the $L^2$-norm distance between models and experiment is of the same order of magnitude for both models. A slight advantage can however be attributed to the SFM-model with a higher $L^2$-norm distance of a few percent up to 23% for the GCFM. This effect is even more pronounced in the Hilbert-Schmidt norm that measures the the distance to the experiment in the fluctuation structure of measured and simulated data. Here the Hilber-Schmidt distance of empirical covariance function of the GCFM to the one of the experiment is consistently almost twice as high as for the SFM.

## VI. STATISTICAL INFERENCE BASED ON THE BOOTSTRAP

In the previous section, we evaluated the total variation and the Gini coefficient or deviation measures for the average behaviour and the fluctuation structure ($L^2$- and HS-norms, respectively) in order to compare simulated data with data from the experiment. This descriptive approach however leaves open the question, to which extent these findings depend on the intrinsic stochastic nature of pedestrian trajectories and to which extent they are due to structural differences between simulated agents in the models and real pedestrians observed in the experiment. In the present section, we describe and apply a simulation based test procedure in order to answer the question, to what extent the observed differences between models and experiment are statistically significant.

### A. Bootstrapping PCA scores

As the basis of our statistical testing procedure, we use the bootstrap over the matrix of principal components from [3, 4]. We now shortly describe the bootstrap approach. Given, e.g., the $i$-th $x$-value of the trajectory over time, $x_i(t)$, the score of this trajectory with respect to the principal component $\xi_j(t)$ is

$$\begin{aligned} s_{ij}^{(x)} &= \langle x_i(t) - \bar{x}(t), \xi_j(t) \rangle \\ &= \left\langle \sum_{l=1}^{K} \underbrace{(c_{i,l} - C_l)}_{\mathbf{\Delta}_{i,l}} \Phi_l(t), \sum_{k=1}^{K} \mathbf{b}_{jk} \Phi_k(t) \right\rangle \\ &= (\mathbf{\Delta}^T \mathbf{W} \mathbf{b}^T)_{i,j} \ . \end{aligned} \tag{27}$$

By construction, the scores $s_{ij}^{(x)}$ and $s_{i,j'}^{(x)}$ are (linearly) uncorrelated for $j \neq j'$. Neglecting potential higher order correlations, we construct a virtual bootstrap sample from the scores of the experimental data by drawing with replacement, for $i, j$ fixed, $s_{i,j}^{(x,\mathrm{boot})}$ from the $N$ samples $s_{i,j}^{(x)}$ of the original scores with respect to the $j$-the principal component $\xi_j(t)$. Doing this independently for $i = 1, \ldots, N$ and $j = 1, \ldots, K$ (remember, in our case $N = 110$ is the number of experimental pedestrian trajectories and $K = 10$ the number of principal components) we obtain the $N \times K$ bootstrap score matrix $\mathbf{s}^{(x,\mathrm{boot})}$. The corresponding bootstrapped trajectories then are

$$x_i^{(\mathrm{boot})}(t) = [\mathbf{s}^{(x,\mathrm{boot})} \Phi(t)]_i + \bar{x}(t), \quad i = 1, \ldots N. \tag{28}$$

Figure 16 shows the x-coordinates plots of pedestrian trajectories by bootstrapped and experimental data.

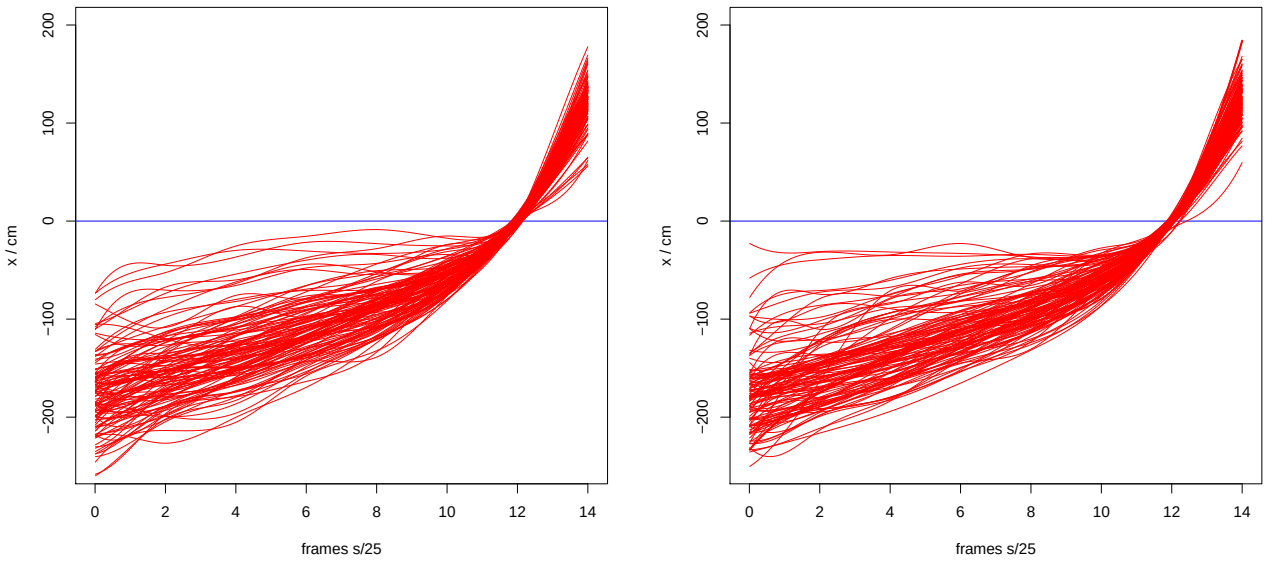


FIG. 16. Plots of x-coordinates of pedestrians by bootstrapped data (left) and experimental data (right).

With this virtual data set, the PCA analysis is then repeated. In particular, we obtain bootstrapped quantities for total variation and Gini index, as well as distance measures for the average behaviour of the actual experiment and its virtual bootstrap replica.

This entire process is then repeated a sufficiently high number of times, such that $p$-values in the range of usual significance levels $\approx 1 - 5\%$ can safely be determined. Here we generate 10 000 bootstrap samples, each containing $N = 118$ virtual trajectories, and thereby obtain a simulated distribution for each of the aforementioned quantities.

Also, we repeat this process for the $y$-coordinate and the $x$ velocity $v_x$.

For statistical testing, we generate two sided confidence intervals for the total variation and the Gini coefficient and left open confidence intervals for the distance measures based on the empirical distributions of the respective

quantities. If the related quantities for the SFM and GCFM model are not contained in these confidence regions, we consider this as a positive test result for a deviation between experiment and model.

### B. Testing Gini indices and total variations

One of the advantages of using this bootstrap technique is to have the opportunity to examine the distributions of Gini indices and the total variations. We compute for every bootstrap sample the Gini indices and total variations by the experimental data for x-coordinates, y-coordinates and x-velocities. Then we are able to compute their empirical cumulative distribution functions (ECDF). Figure 17 shows the ECDF of Gini indices and total variations of x-coordinates by bootstrapped experimental data. The blue lines shows the values of Gini index and total variation by original experimental data. The corresponding $p$-values, i.e. the critical level of statistical significance where the difference between model and experiment just becomes singificant, are calculated on the basis of two-sided confidence regions of the bootstrapped distribution. The $p$-values are are summarized in Table IV. Note that $p$-values below $10^{-3}$ become numerically unreliable for $10^4$ bootstrap samples and are set to zero.

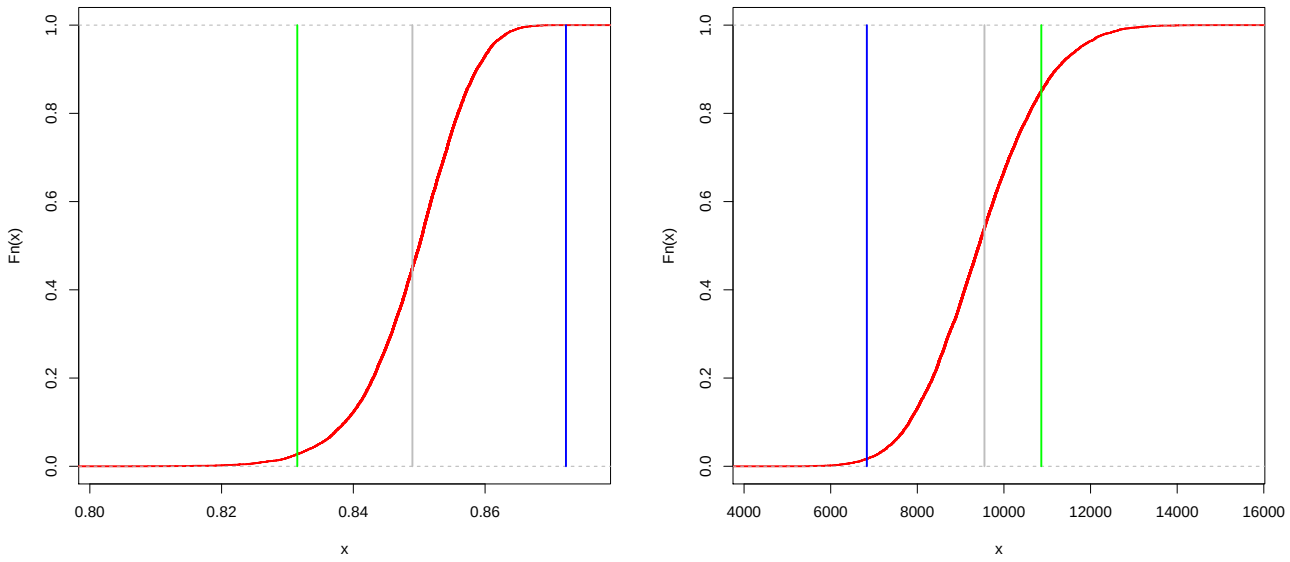


FIG. 17. ECDF of Gini indices (left) and ECDF of total variation (right) from bootstrapped experimental data. Green, grey and blue vertical lines mark the values for the SFM, experiment and GCFM, respectively.

| **p-values for Gini index** | | |
|---|---|---|
| | EXP/GCFM | EXP/SFM |
| $x$-position | 0 | 0.055 |
| $y$-position | 0.610 | 0.007 |
| $x$-velocities | 0 | 0 |

| **p-values for TotalVar** | | |
|---|---|---|
| | EXP/GCFM | EXP/SFM |
| $x$-position | 0.034 | 0.297 |
| $y$-position | 0 | 0 |
| $x$-velocities | 0 | 0 |

TABLE IV. The p-value of Gini index and total variations by bootstrapped experimental data.

The $p$-values in Table IV show that statistical testing reveals significant differences between experiment and model with respect to several Gini indices and total variations. Only the concentration measure of the GCFM and the total variation of the SFM do not produce significant differences (significance level 5%).

### C. Tests based on deviation measures

We are now interested to measure the deviations between bootstrapped and experimental data. Firstly we compute for every bootstrap sample the $L^2$ norm of the difference between the mean trajectory of the bootstrap sample based on the virtual experimental data and the mean trajectory of the experiment. In this way we obtain a empirical distribution of the $L^2$-norm distance due to natural fluctuation inside the experiment. This is then compared with the $L^2$-norm distance of average trajectories between the experiment and the SFM and GCFM model. The same procedure is also carries through for the Hilber-Schmidt distance between the estimated correlation functions, see Figure 18.

Again, $p$-values are calculated as in the previous subsection, however this time we have to use one-sided regions of confidence for statistical testing. The $p$-values are displayed in Table V.

| **p-values for $L^2$ norm** | | |
|---|---|---|
| | EXP/GCFM | EXP/SFM |
| $x$-position | 0 | 0 |
| $y$-position | 0.512 | 0.576 |
| $x$-velocities | 0 | 0 |

| **p-values for HS norm** | | |
|---|---|---|
| | EXP/GCFM | EXP/SFM |
| $x$-position | 0.122 | 0.434 |
| $y$-position | 0 | 0 |
| $x$-velocities | 0 | 0 |

TABLE V. The p-values for $L^2$ norm and Hilbert-Schmidt norm .

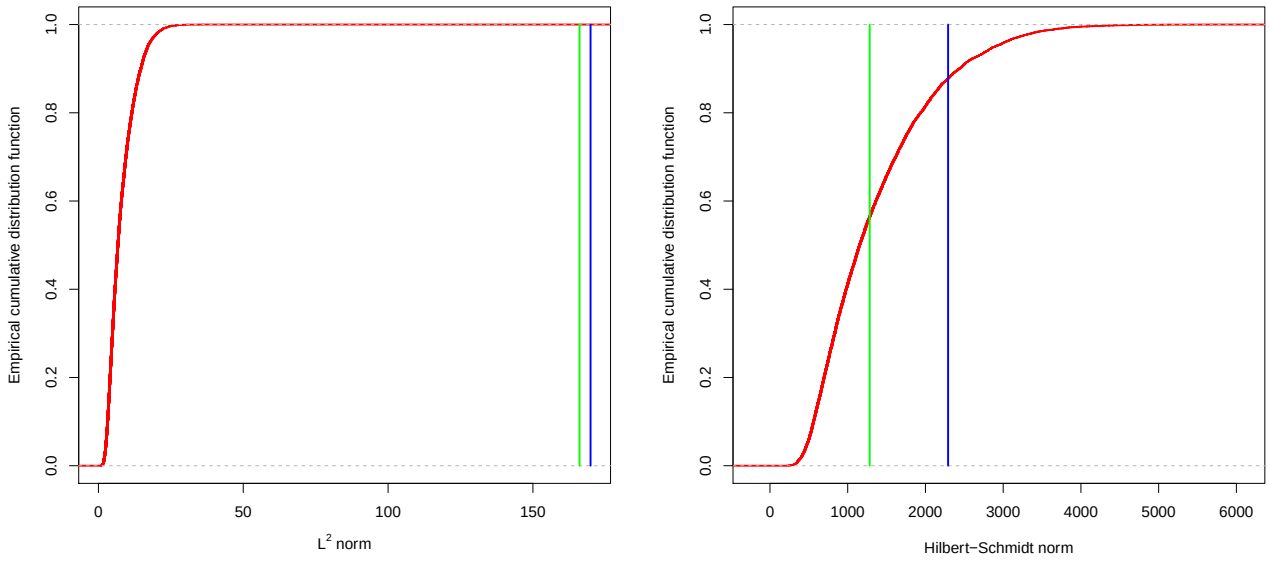


FIG. 18. The ECDF of the $L^2$-norm difference of average $x(t)$ values (left) and the Hilbert Schmidt (HS) norm difference between covariance functions of $x(t)$ fluctuations of experimental and bootstrapped data. Green and blue vertical lines show $L^2$- and HS-norm distance between the experiment SFM and GCFM models respectively.

All statistical tests of the $L^2$-norm distance between the average $x$-values and $v_x$-values of the experiments and the models are highly significant. We find thus a clear indication that model and experiment can be statistically distinguished. Not unexpectedly, the situation is different for the average of the $y$-values over time. Here, due to the axial symmetry of the experimental set up, no major differences of the average $y$-trajectory can be expected. This also shows that the slight asymmetry in the average $y$-trajectory in the experimental data is not statistically significant.

With regard to the fluctuation structure, the $x$-position fluctuations encoded by the empirical correlation function can not be easily distinguished between the SFM model and the experiment. The difference between the fluctuation of the $x$-trajectories of the GCFM and the experiment also shows a very poor $p$-value of $\approx 12\%$, which is not significant when compared to the usual 5%-level of significance. All other fluctuation structures significantly differ between the experiment and the models.

## VII. SUMMARY

The functional PCA has been applied as a diagnostic tool to assess model quality for agent based simulations of pedestrian flows with respect to average behaviour and beyond. Here we applied it to experimentally measured pedestrian trajectories passing through a bottleneck and agent trajectories simulated by the SFM and GCFM.

Already in the analysis of mean flow behaviour, the PCA revealed considerable and statistically significant deviation of both models from the experiment. In the $x$-direction and the $x$-velocity component, the SFM and the GCFM predict slower progress and lower velocities leading to a longer dwell time before the bottle neck, as experimentally observed, although total through flow has been calibrated. This effect is more pronounced for the GCFM average behaviour so that the SFM model reproduces the average behaviour of the experiment – for the given set of parameters – in a relatively better way.

Coming to the statistical variations simulated in the SFM for $x$-position and velocity over time, we find a quite reasonable match in the qualitative behaviour (the PCA mode shapes) of the $x$- and $y$-position over time. A certain deviation in the quantitative variation strength and the velocity variation shapes is observed as well. Again the SFM predictions are a little closer, when measured in terms of the deviation in the total variation. Also, the concentration of variability to dominating modes is under estimated by the SFM and over estimated by the GCFM for the $x$-variations, while in the velocity variations both models show a higher degree of concentration as compared with the experiment.

Summarizing the PCA gives none of the models a clear "pass", as the SFM and the GCFM both significantly differ from the experiment. The SFM however performs relatively better than the GCFM, which is mostly due to a gradually better prediction of the average $x$-positions and $x$-velocities.

Caution is needed when applying these (and presumably also other) models to evacuation studies, as the evidently do not capture all features of real life pedestrian flows, as has been shown by our functional data analysis. The overall picture of all the qualitative metrics derived from the PCA however slightly favours the SFM as the more accurate model over the GCFM, given our set of model parameters.

In this case study, applying functional PCA for the first time to pedestrian flows, we have thus shown that it is in fact a useful tool to benchmark and statistically test agent based pedestrian flow models. Given the amount of deviation between experiment and model, it is certainly of interest to use this methodology for the future refinement of pedestrian flow models and for the critical assessment of models used by practitioners.

## ACKNOWLEDGMENTS

We would like to thank Stefan Rosbach for his preparatory work on the functional PCA analysis for pedestrian data.

[1] Bauer, H., Probability Theory, de Gruyter 1995.
[2] Chraibi, M., Seyfried, A., and Schadschneider, A., The generalized centrifugal force model for pedestrian dynamics, *Phys. Rev. E* **82** (2010) 046111.
[3] Diaconis, P. and Efron, B., Computer-intensive methods in statistics. Scientific American, **248** No. 5 (1983) 116–130.
[4] Fisher, A., Caffo, B., Schwartz, B. and Zipunnikov, V., Fast, Exact Bootstrap Principal Component Analysis for $p > 1$ million, arXiv:1405.0922v3.
[5] Helbing, D., Collective phenomena and states in traffic and self-driven many-particle systems, *Comp. Mater. Sci.* **30** (2004) 180–187.
[6] Helbing, D. and Molnár, P., Social force model for pedestrian dynamics, *Phys. Rev. E* **51** (1995) 4282–4286.
[7] Hoogendoorn, S. P. and Daamen, W., Microscopic Parameter Identification of Pedestrian Models and its Implications to Pedestrian Flow Modeling (Transporttation Research Board Annual Meeting, 2006).
[8] Jian, M., Weiguo, S., Jun, Z., Siuming, L., and Guahgxuan, L., k-Nearest-Neighbor interaction induced self-organized pedestrian counter flow, *Physica A: Statistical Mechanics and its Applications* **389** (2010) 2101–2117.
[9] Lakoba, T. I., Kaup, D. J., and Finkelstein, N. M., Modifications of the Helbing-Molnár-Farkas-Vicsek social force model for pedestrian evolution, *Simulation* **81** (2005) 339–352.
[10] Molnár, P., Modellierung und Simulation der Dynamik von Fußgängerströmen, Ph.D. Thesis. University Stuttgart 1996.
[11] Nishinari, K., Sugawara, K., and Kaza, Modelling of self-driven particles: Foraging ants and pedestrians, *Physica A* **372** (2006) 132–141.
[12] Parisi, D. R. and Dorso, C. O., Morphological and dynamical aspects of the room evacuation process, *Physica A* **385** (2007) 343–355.
[13] Pipes, L. A., An operational analysis of traffic dynamics, *J. Appl. Phys.* **24** (1953) 274 – 281.

[14] Ramsay, J., Hooker, G. and Graves, S. , Functional Data Analysis with R and Matlab, UseR! Series, Springer Dortrecht Heidelberg London New York, 2009.
[15] Ramsay, J. and Silverman, B., Functional Data Analysis, Springer Verlag New York, 2005.
[16] Seyfried, A. and Schadschneider, A., Fundamental Diagram and Validation of Crowd Models, in *Cellular Automata*, eds. Umeo, H., Morishita, S., Nishinari, K., Komatsuzaki, T., and Bandini, S., *Lecture Notes in Computer Science*, Vol. 5191/2008 (Springer, Berlin Heidelberg, 2008), pp. 563–566, doi:10.1007/978-3-540-79992-4.
[17] Seyfried, A. and Schadschneider, A., Empirical results for pedestrian dynamics at bottlenecks, in *Parallel Processing and Applied Mathematics*, eds. Wyrzykowski, R., Dongarra, J., Karczewski, K., and Wasniewski, J., *Lecture Notes in Computer Science*, Vol. 6068 (Springer, Berlin Heidelberg, 2010), pp. 575–584, `http://dx.doi.org/10.1007/978-3-642-14403-5_62`.
[18] Seyfried, A., Steffen, B., and Lippert, T., Basics of modelling the pedestrian flow, *Physica A* **368** (2006) 232–238.
[19] Shiwakoti, N., Sarvi, M., Rose, G., and Burd, M., Animal dynamics based approach for modelling pedestrian crowd egress under panic conditions, *Transportation and Traffic Theory* **17** (2011) 438–461.
[20] Steffen, B. and Seyfried, A., Methods for measuring pedestrian density, flow, speed and direction with minimal scatter, *Physica A* **389** (2010) 1902–1910.
[21] W. J. Yu, R. Chen, L. Y. Dong and S. Q. Dai, Centrifugal force model for pedestrian dynamics, *Phys. Rev. E*, **72** (2005) p. 026112.
[22] Zhang, J., Klingsch, W., Schadschneider, A., and Seyfried, A., Transitions in pedestrian fundamental diagrams of straight corridors and t-junctions, *J. Stat. Mech.* (2011).